UNIVERSITY OF AMSTERDAM

UvA-DARE (Digital Academic Repository)

Revealing and Quantifying the Three-Dimensional Nano- and Microscale Structures in Self-Assembled Cellulose Microfibrils in Dispersions

Mohan, S.; Jose, J.; Kuijk, A.; Veen, S.J.; van Blaaderen, A.; Velikov, K.P.

DOI
10.1021/acsomega.7b00536

Publication date
2017

Document Version
Final published version

Published in
ACS Omega

License
Other

Link to publication

Citation for published version (APA):
Mohan, S., Jose, J., Kuijk, A., Veen, S. J., van Blaaderen, A., & Velikov, K. P. (2017). Revealing and Quantifying the Three-Dimensional Nano- and Microscale Structures in Self-Assembled Cellulose Microfibrils in Dispersions. *ACS Omega*, *2*(8), 5019-5024. https://doi.org/10.1021/acsomega.7b00536

General rights
It is not permitted to download or to forward/distribute the text or part of it without the consent of the author(s) and/or copyright holder(s), other than for strictly personal, individual use, unless the work is under an open content license (like Creative Commons).

Disclaimer/Complaints regulations
If you believe that digital publication of certain material infringes any of your rights or (privacy) interests, please let the Library know, stating your reasons. In case of a legitimate complaint, the Library will make the material inaccessible and/or remove it from the website. Please Ask the Library: https://uba.uva.nl/en/contact, or a letter to: Library of the University of Amsterdam, Secretariat, P.O. Box 19185, 1000 GD Amsterdam, The Netherlands. You will be contacted as soon as possible.

UvA-DARE is a service provided by the library of the University of Amsterdam (https://dare.uva.nl)

Download date:14 Oct 2026

This is an open access article published under an ACS AuthorChoice License, which permits copying and redistribution of the article or any adaptations for non-commercial purposes.

ACS OMEGA

Article

http://pubs.acs.org/journal/acsodf

Revealing and Quantifying the Three-Dimensional Nano- and Microscale Structures in Self-Assembled Cellulose Microfibrils in Dispersions

Srivatssan Mohan,[†] Jissy Jose,[‡,∥] Anke Kuijk,[‡,⊥] Sandra J. Veen,[‡,#] Alfons van Blaaderen,[†] and Krassimir P. Velikov*[,†,‡,§]

[†]Soft Condensed Matter, Debye Institute for NanoMaterials Science, Utrecht University, Princetonplein 5, 3584 CC Utrecht, The Netherlands

[‡]Unilever R&D Vlaardingen, Olivier van Noortlaan 120, 3133 AT Vlaardingen, The Netherlands

[§]Institute of Physics, University of Amsterdam, Science Park 904, 1098 XH Amsterdam, The Netherlands

Supporting Information

ABSTRACT: Cellulose microfibrils (CMFs) are an important nanoscale building block in many novel biobased functional materials. The spatial nano- and microscale organization of the CMFs is a crucial factor for defining the properties of these materials. Here, we report for the first time a direct three-dimensional (3D) real-space analysis of individual CMFs and their networks formed after ultrahigh-shear-induced transient deagglomeration and self-assembly in a solvent. Using point-scanning confocal microscopy combined with tracking the centerlines of the fibrils and their junctions by a stretching open active contours method, we reveal that dispersions of the native CMFs assemble into highly heterogeneous networks of individual fibrils and bundles. The average network mesh size decreases with increasing CMF volume fraction. The cross-sectional width and the average length between the twists in the ribbon-shaped CMFs are directly determined and compared well with that of fibrils in the dried state. Finally, the generality of the fluorescent labeling and imaging approach on other CMF sources is illustrated. The unique ability to quantify in situ the multiscale structure in CMF dispersions provides a powerful tool for the correlation of process−structure−property relationship in cellulose-containing composites and dispersions.

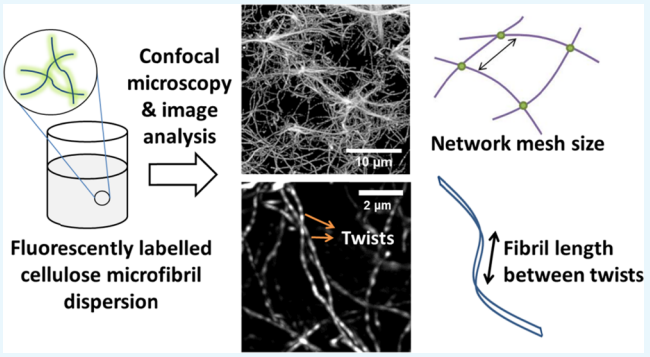

INTRODUCTION

Filamentous biopolymer-based networks are ubiquitous in nature and play a crucial role in maintaining the structural integrity of living systems. Cellulose forms an important class of fibrillar biopolymer systems owing to its specific molecular structure and defined hierarchical order that lead to many interesting properties.[1] The cellulose-based nanoscale materials derived from cellulose microfibrils (CMFs), also referred to as nanofibrils (Figure S1),[2] are of great interest for several applications owing to their shape anisotropy, high strength, and chirality.[3−6] Recently, there has been a strong interest in the three-dimensional (3D) CMF networks driven by their potential use in many advanced biobased materials such as a transparent paper,[7] a conductive paper,[8] functional aerogels,[9−12] implants and scaffolds in tissue engineering,[13] and high-strength structural composites.[14] The nature of assembly and organization of CMFs in dispersions often prepared by high-shear defibrillation or deagglomeration using ultrahigh-pressure homogenization or microfluidization process holds the key to attain the desired properties of the composite materials derived from them.[15,16] Such high-energy processes allow transient deagglomeration followed by the self-assembly of the CMF, which can be modulated by controlling their interparticle interactions.[17] Methods for studying CMF dispersion in their native, nondried form are much needed to understand the nano- and microscale organization in these materials.

The morphology of CMF from different sources has been studied using high-resolution imaging techniques such as transmission electron microscopy (TEM) and atomic force microscopy (AFM).[18−20] A fundamental limitation of studying CMF dispersions using TEM and AFM is that these methods are more relevant for understanding the properties of the fibrils in their dry state. These methods can be prone to the generation of artifacts resulting from the sample preparation processes.[18] Kaushik et al. had used cryo-TEM to study the nanocrystallites of cellulose in their suspension form, and it revealed marked differences with the dried forms.[4] The structure and properties of 3D networks of the self-assembled

Received: April 30, 2017
Accepted: June 13, 2017
Published: August 28, 2017

Downloaded via UNIV AMSTERDAM on October 27, 2020 at 15:40:17 (UTC).
See https://pubs.acs.org/sharingguidelines for options on how to legitimately share published articles.

© 2017 American Chemical Society

DOI: 10.1021/acsomega.7b00536
ACS Omega 2017, 2, 5019−5024

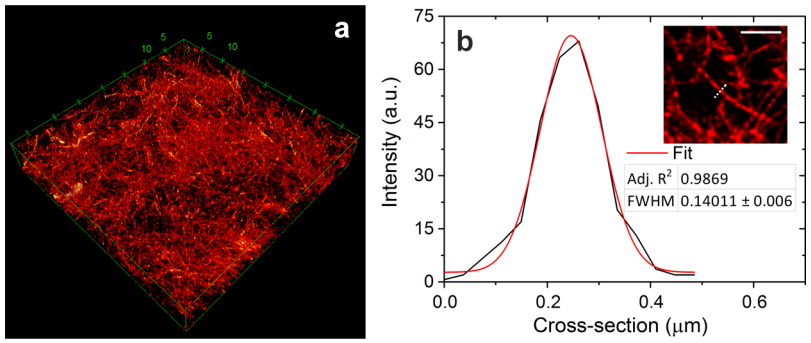

Figure 1. (a) 3D confocal image (38.19 × 38.19 × 6.76 μm^3) of the CMF network in the BC pellicle. (b) Intensity profile along a fibril cross-section indicating the resolution of imaging. Inset: maximum intensity projection of a section of (a). Scale bar: 2 μm.

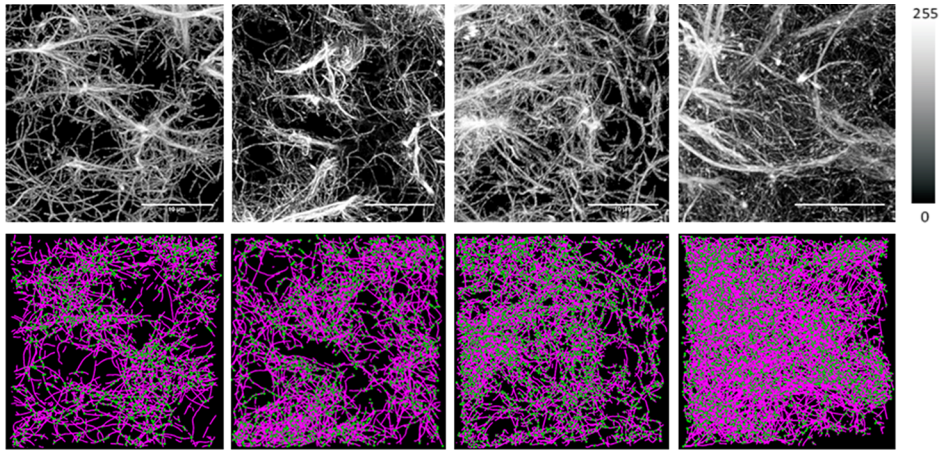

Figure 2. Maximum intensity projection of 3D confocal images (up) of CMF networks at different volume fractions [left to right: 0.11% (30.22 × 30.22 × 5.98 μm^3), 0.13% (30.62 × 30.62 × 5.85 μm^3), 0.18% (30.22 × 30.22 × 5.98 μm^3), and 0.22% (24.02 × 24.02 × 9.49 μm^3) ϕ] and their respective 3D reconstruction images (purple = fibrils, green = fibril junctions). Scale bar: 10 μm.

CMFs in dispersions, however, could markedly differ between those that were never-dried and those that have been in a dried state.[21] Also, most of the applications of CMFs involve their processing in a never-dried hydrated state or in various solvents, and hence, it is of great interest to study the 3D nano- and microstructures of these CMFs in their "wet" state. Previous reports on imaging cellulose in the native "wet" state include comparing direct visualization of CMFs in plant cell walls using confocal microscopy along with image deconvolution with total internal reflection microscopy and direct stochastic optical reconstruction microscopy.[22] However, the contrast of fibrils in their images was poor, probably because of the limited noncovalent attachment of the dye to cellulose. Fluorescent labeling of the native CMFs has been demonstrated previously by Helbert et al. on bacterial cellulose (BC) that has been homogenized by a low-energy blender, which does not create conditions for the transient deagglomeration of the microfibrils.[23] Zammarano et al. have used a similar labeling approach to reveal the interface in cellulose−polymer composites.[24] The functional properties of the composite materials are governed by both the nano- and microscale spatial and orientational organizations of the reinforcing fibrils, which are in turn influenced by the processing conditions.[16] Considering the rapid developments in the utilization of CMFs in various nanostructured composite materials, it is important to perform a 3D real-space analysis of their assembled structure, which is often a precursor for the final material,[9−12,25,26] to reveal and quantify the mesoscale organization.

RESULTS AND DISCUSSION

In this study, CMFs from different sources were fluorescently labeled with fluorescein isothiocyanate (FITC) to visualize and observe their microstructure using confocal microscopy. FITC reacts with hydroxyl groups along the surface of CMFs, leading to covalent attachment. Imaging contrast was improved by having a dye grafted to the fibril surface compared with that of a physically adsorbing dye that can partially remain in the solvent (Figure S2). The CMFs sourced from bacteria are a pure form of cellulose, free from lignin and hemicellulose;[27] hence, they serve as a good model system to investigate the properties of 3D networks of the self-assembled CMFs. The refractive index (RI) mismatch between the sample medium and the objects in it and the imaging objective leads to deterioration of the point spread function (PSF), which becomes more pronounced with increasing the depth of focus into the sample volume in the case of 3D imaging.[28] This effect was reduced by dispersing the CMF in dimethyl sulfoxide (DMSO) where the RI difference is lesser than that in water. Scattering within the sample is lowered considerably, leading to further improvement in the imaging quality. During imaging, no change in the network structure of the CMFs was detected as their motion was topologically constrained in the range of concentrations analyzed. The network structures of samples below 0.05% volume fraction (ϕ) obtained by simple dilution (i.e., without

DOI: 10.1021/acsomega.7b00536
ACS Omega 2017, 2, 5019−5024

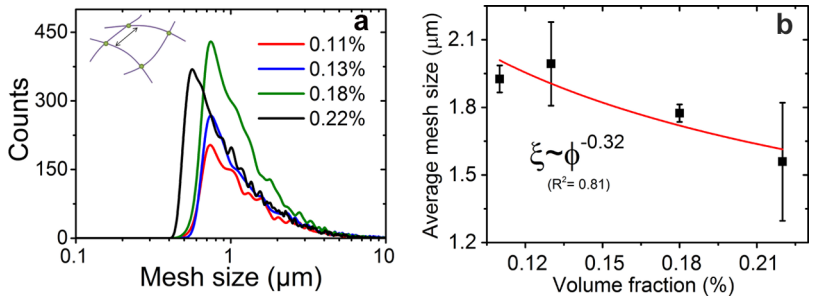

Figure 3. (a) Distribution of the mesh size of CMF networks at different volume fractions. (b) Average mesh size per unit volume with respect to the volume fraction of the CMF network.

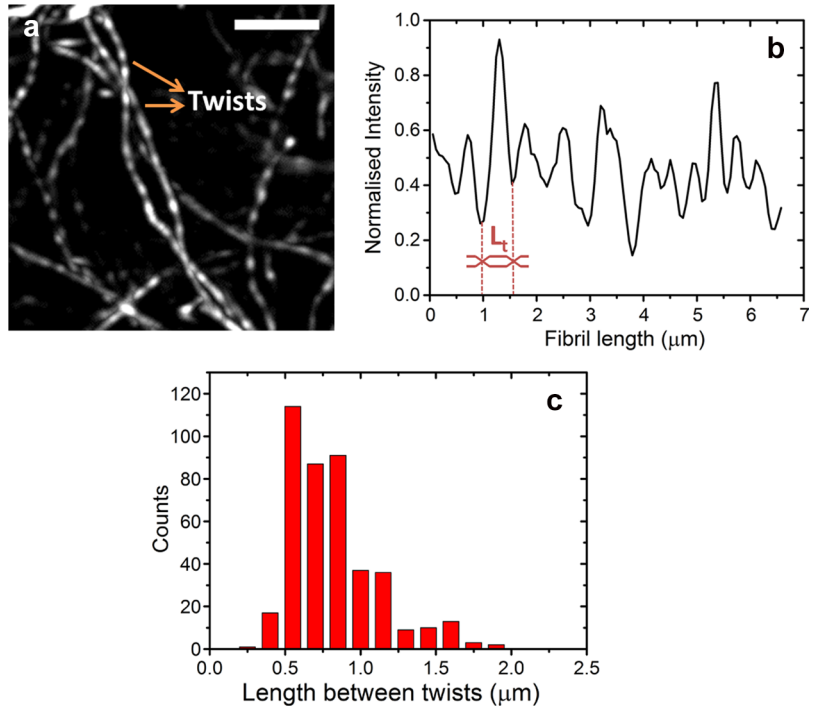

Figure 4. (a) Maximum intensity projection of a 3D confocal image (7.62 × 7.62 × 7.68 μm^3), showing alternating bright and dark segments along the fibril contours (scale bar: 2 μm). (b) Intensity profile of a representative fibril. (c) Distribution of fibril lengths between the twists analyzed from a 3D confocal image.

high shear) could not be imaged as the ends of some fibrils started to dangle owing to the loss of topological constraints (see Movie M1). Figure 1a shows a deconvoluted 3D image of the BC pellicle (i.e., the 3D network of CMF before high-shear deagglomeration) imaged with confocal microscopy. Deconvolution using a theoretical PSF was done to improve the images. The fine network structure of individual CMFs inherent in these pellicles can be seen clearly. We could estimate the width of fibrils from the intensity profile along its cross-section (Figure 1). By applying a Gaussian fit (Figure 1b) to the intensity profile along a fibril cross-section, we obtained a full-width at half maximum of 140 nm, which is within the range of fibril widths determined by using electron microscope from our studies (Figure S1) and as reported by others.[29,30]

When subjected to very high shear homogenization by microfluidization, the CMFs experience transient deagglomeration, which allow the fibrils to self-assemble in a different way. This self-assembly process can be strongly influenced by the presence of an adsorbing polymer that controls interparticle interactions.[17] The CMF dispersed in DMSO was imaged at different volume fractions (made by concentrating a 0.11% ϕ stock dispersion), as shown in Figure 2. One can see that at higher volume fractions the networks appear denser and bundling of fibrils is more evident. The microstructure is heterogeneous with the presence of both individual and bundles of fibrils. Voids are present. Using a stretching open active contours (SOAC) algorithm,[31] the centerlines of the fibrils were traced, and the network was reconstructed to obtain their coordinates in 3D along with that of the fibril contacts (junctions). Closely packed fibrils that appear as one thick bundle are traced as single fibrils owing to the lack of sufficient resolution parting one fibril from another.

Owing to the heterogeneous nature of the network microstructure, the fibril length between the subsequent junctions, which directly relates to the mesh size, ξ, of the network,[32] has a broad distribution range as shown in Figure 3a for different volume fractions. Figure 3b shows the plot of the average mesh size per unit volume. It is interesting to note that some of these values lie in the same range irrespective of the CMF volume fraction.

It is established generally that the mesh size of densely connected filamentous polymer networks follows a power-law

DOI: 10.1021/acsomega.7b00536
ACS Omega 2017, 2, 5019−5024

relationship with concentration with an exponent of −0.5; $\xi \approx \phi^{-0.5}$.[32] However, the behavior of CMF networks differs as the network is formed from the components that exert strong attractions on each other, which breaks down to flocs (not to individual fibrils) upon dilution or moderate shear.[33] We do observe that the average mesh size decreases with increasing volume fraction as $\xi \approx \phi^{-0.32}$. The smaller exponent is the result accounted by the presence of voids in the network, which decreases both in size and in number concentration with increasing volume fractions of CMFs.

The amount of shear applied plays a definite role in governing the microstructure of the network formed in the case of CMFs.[34] The samples were prepared by concentrating 0.11% ϕ stock dispersions. Therefore, the microstructure formed by 0.11% sample would be inherited to the rest of the samples. This is clearly reflected in the mesh size distributions of 0.11, 0.13, and 0.18% ϕ samples, which fall in the same range. The measured fibril count could be higher as some bundles get classified as single fibrils in the image reconstruction process. It is also to be noted that the image reconstruction process is not artifact-free; the results represent a quantitative analysis of the CMF network microstructure (Figure S3).

An interesting observation that can be made from these images is the appearance of alternating bright and dark segments along the length of the fibrils, as shown in Figure 4a. This corresponds to the twists inherent in these ribbon-shaped fibrils. The variation in intensity along a part of a fibril contour is shown in Figure 4b for a fibril marked in Figure 4a. The darker segments along the fibril contour, which correspond to valleys (or minima) in the intensity profile, represent twists. From the 3D intensity profile, the distances between the subsequent minima reveal the fibril length between the twists (L_t). Figure 4c shows the distribution ranging from 0.3 to 2 μm, with an average value of 0.73 μm from analyzing about 80 fibrils of varying widths. This value is slightly smaller than the one obtained by analyzing the TEM images (see Figure S4) of the CMF dried from the aqueous media, from which we determined an average length of 0.85 μm per twist. The reason for this difference might be due to gradual and natural twisting of CMFs in the dispersed state compared to the sharp and segmented twists in the dried fibrils, as proposed by Hanley et al.[19]

It is evident from our confocal images that the CMFs are twisted gradually, unlike in the TEM images of the fibrils in the dried state. Our L_t analysis results are also consistent with the ones reported by Colvin, which were found to be about 0.7 to 1 μm for single dry fibrils based on the TEM observations.[35] He also reported a significant variation in the pitch of the twists even within a single pair of CMFs. However, we are unable to comment on the uniformity of the interval of occurrence of twists as we have taken into account the fibrils of varying widths ranging from single fibrils to bundles in our analysis. The mechanism behind the twisting of cellulose is still debated.[36]

To demonstrate the generality of our approach, we fluorescently labeled CMF dispersions obtained from the plant biomass materials. Sugarcane fiber and citrus fiber, which are by-products from the production of sugar and pectin, respectively, were selected as examples (Figure 5). These two sources contain not only cellulose but also soluble polymers such as pectin and hemicellulose, which are typically present in the primary cell walls of the plant.[27] A comparison of the microstructures of these two sources of CMFs dispersed in water is shown in Figure 5. The citrus fiber dispersion, which

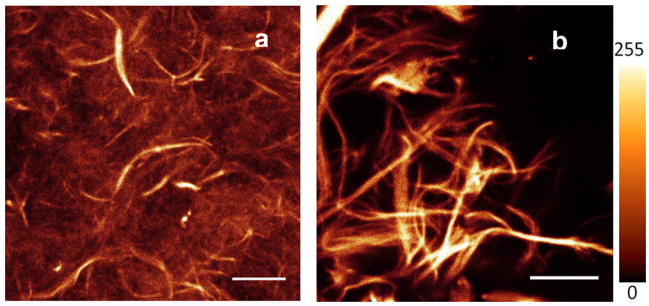

Figure 5. 2D confocal images of CMF networks in (a) citrus fiber and (b) sugarcane fiber dispersions in water. Scale bar: 5 μm.

contains a higher level of soluble biopolymers, shows a more homogeneous CMF network. The diffusive background could originate from some degree of covalent attachment of the FITC molecules to the soluble polymers like pectin. The observed more homogeneous CMF networks are similar to the case of CMFs in the presence of adsorbing charge polymers (e.g., CMC[17]). The CMF networks derived from the sugarcane appear to behave more like dispersion of pure CMFs, which is in line with the very higher content of cellulose (as indicated by the supplier).

CONCLUSIONS

In conclusion, we demonstrate the first direct 3D visualization and quantitative analysis of individual CMFs, bundles, and their networks in dispersion. We obtained the mesh size distribution of the networks at different volume fractions. Twists inherent in the microfibrils were clearly identified from the confocal images. The average length between the twists was found to be slightly greater in the "wet" state when compared to that in the dried fibrils. The ability to perform a quantitative 3D real-space analysis will greatly advance the understanding of structure−mechanics relations in nanoscale fibrillar networks.[37] Future work in this direction will focus on studying the effects of shear on the network structure of CMFs (see Figure S5).

EXPERIMENTAL SECTION

Materials. Sugarcane fibers (UltraCel, WT-11989) were obtained from Watson Inc. Citrus fibers (HERBACEL-AQ Plus, type N) were obtained from Herbafood. The BC microfibrils in the form of pellicles of the strain *Acetobacter* were sourced from a commercial Nata de coco product (Cozzo Food Industries, Malaysia).

Sample Preparation. Syrup from the product was discarded, and the BC pellicles were immersed in a bath of 0.1 M NaOH solution and then washed thoroughly with deionized (DI) water (Millipore Direct-Q3). The washed pellicles were immersed in DI water and broken down using a hand blender (Braun 4185545). The resulting BC slurry was then subjected to eight washing cycles involving vacuum filtration and redispersion in DI water, to remove soluble impurities. After this, it was passed through a shearing device called Microfluidizer M-110S (Microfluidics Corp) operating at a pressure of 1200 bar to obtain a macroscopically homogeneous dispersion. The volume fraction (ϕ) of BC in the dispersion was determined gravimetrically as the average of three samples from which water was evaporated at 40 °C under a pressure of 40 mbar in a vacuum oven (Memmert Celcius), using the density value of CMFs as 1.5 g/mL.[38]

DOI: 10.1021/acsomega.7b00536
ACS Omega 2017, 2, 5019−5024

CMFs were fluorescently labeled with FITC by adopting the mechanism reported by Nielsen et al.[39] for charged cellulose nanocrystals. In a typical reaction, 100 mg of FITC (≥90%, Sigma-Aldrich) dissolved in 5 mL of 0.1 M NaOH solution was added to 250 mL of 0.5 wt % CMF dispersed in 0.1 M NaOH. This mixture was kept under constant stirring using a magnetic stirrer and allowed to react for 4 days under no exposure to visible light. After the reaction, the labeled CMF dispersions were purified by washing with 0.1 M NaOH and then with DI water by repeated centrifugation (Hettich ROTANTA 460R) at 3566 relative centrifugal field (RCF) for 20 min followed by redispersion in DI water until the dispersion was colorless and showed no background fluorescence when observed under a fluorescence microscope. The CMF dispersions in DMSO (≥99.9% ACS reagent, n_D 1.479, Sigma-Aldrich) were prepared by gradual solvent exchange facilitated by repeated centrifugation, decantation, and addition of DMSO, thus avoiding drying of the fibrils. The RI of the supernatant was measured using an Abbe refractometer (ATAGO NAR 3T) as n_D 1.4772 at 20 °C in the final dispersion, which corresponds to 99% DMSO content. The CMF dispersion in DMSO was then run once through a Microfluidizer operating at 1200 bar in order for the network microstructure to re-evolve in DMSO. From the stock dispersion, samples at different weight % were prepared by either dilution (by solvent addition followed by mixing using a universal small shaker at 2500 rpm) with DMSO or concentration (by centrifugation at 3566 RCF for 20 min). The CMFs from other sources like citrus fiber (30−50 wt % cellulose) and sugarcane fiber (90 wt % cellulose) were labeled with FITC following the same procedure. They were imaged in water.

Confocal Microscopy and Image Analysis. For confocal imaging, the FITC-labeled CMF dispersions were transferred slowly into an imaging cell of 5 mm diameter with a depth of 3 mm to avoid shearing the fibrils. A Leica SP8 microscope (Leica Microsystems, Germany) with a confocal 100 × NA 1.4 oil (n = 1.515) immersion objective lens with 495 nm excitation was used to image the samples. The 3D images were obtained by scanning a series of 2D images while moving the microscope stage in the axial direction. The imaging was done in 24-bit 1024 × 1024 pixel format with an average voxel size of 30 × 30 × 130 nm^3, within the ideal sampling interval according to the Nyquist criterion.[40] The obtained 3D fluorescence stack images were deconvoluted by applying the theoretical PSF calculated from microscopy parameters, using a classic maximum likelihood estimation method.[41] This process was carried out using commercially available software (Huygens Professional 15.05, Scientific Volume Imaging). For quantitative analysis, we used an open-source program called SOAX[42] (version: 3.5.9), which tracks the centerlines of filamentous networks and their junctions by the SOAC method.[31] Prior to analysis, the deconvoluted confocal microscopy images were downsized to 8-bit 512 × 512 pixel format, contrast-enhanced using ImageJ 1.49k, and then the voxel size was made isotropic in all directions using the SOAX program. Two main parameters that influence the extraction process are the ridge threshold parameter (τ) that specifies the minimum intensity to initialize an SOAC and the stretch factor (K_{str}) that determines how easily the initialized SOAC evolves. The optimal parameters for the extraction process, τ and K_{str}, were obtained from the best SOAC program by varying these parameters over a range for a representative image. From the list of candidate extraction results of optimal parameters, we manually selected a result that matched closely with the original image. We used τ and K_{str} values in the range of 0.005−0.01 and 0.10−0.20, respectively, depending on the fibril volume fraction. The confocal images were further contrast-enhanced for display.

Analysis of the Fibril Length between the Twists. The periodic variation in intensity along the fibril contour observed in confocal fluorescence images was correlated with the twists inherent in the ribbon-shaped fibrils of the BC. The images were reconstructed using SOAX to obtain the foreground intensity along the centerlines of the fibrils. The distances between the subsequent minima in the intensity profile data along the fibril length in 3D reveal the distance between the twists. The analysis was carried out in Origin 9.1 using the peak analyzer option to obtain the distance between the subsequent minima. Prior to the analysis, the intensity profile obtained from SOAX was smoothened by an adjacent averaging method to not take into account the small fluctuations arising from imaging noise.

■ ASSOCIATED CONTENT

Supporting Information

The Supporting Information is available free of charge on the ACS Publications website at DOI: 10.1021/acsomega.7b00536.

Width distribution of dried CMFs determined using TEM, comparison of noncovalently labeling, magnified portions of confocal and SOAX-rendered images, twists determined using TEM, effect of simple shear (PDF)

Movie of dangling fibrils (AVI)

■ AUTHOR INFORMATION

Corresponding Author

*E-mail: krassimir.velikov@unilever.com (K.P.V.).

ORCID

Krassimir P. Velikov: 0000-0002-8838-1201

Present Addresses

[‖]Department of Chemistry, University of Pennsylvania, Philadelphia, Pennsylvania 19104, United States (J.J.).

[⊥]Agrotechnology and Food Sciences, Wageningen UR, Bornse Weilanden 9, 6708 WG Wageningen, The Netherlands (A.K.).

[#]Electric Ant Lab, Panamalaan 4K, 1019 AZ Amsterdam, The Netherlands (S.J.V.).

Author Contributions

The manuscript was written through contributions from all authors. All authors have given approval to the final version of the manuscript.

Notes

The authors declare no competing financial interest.

■ ACKNOWLEDGMENTS

We thank G. H. Koenderink and C. Storm for their useful discussions. This work was a part of the research program of the Foundation for Fundamental Research on Matter (FOM) and was supported by NanoNextNL.

■ REFERENCES

(1) Klemm, D.; Heublein, B.; Fink, H.-P.; Bohn, A. Cellulose: Fascinating Biopolymer and Sustainable Raw Material. *Angew. Chem., Int. Ed.* **2005**, *44*, 3358−3393.

(2) Chinga-Carrasco, G. Cellulose fibres, nanofibrils and microfibrils: The morphological sequence of MFC components from a plant physiology and fibre technology point of view. *Nanoscale Res. Lett.* **2011**, *6*, 417.

DOI: 10.1021/acsomega.7b00536
ACS Omega 2017, 2, 5019−5024

(3) Deng, J.; Li, J.; Chen, P.; Fang, X.; Sun, X.; Jiang, Y.; Weng, W.; Wang, B.; Peng, H. Tunable Photothermal Actuators Based on a Pre-programmed Aligned Nanostructure. *J. Am. Chem. Soc.* **2016**, *138*, 225−230.
(4) Kaushik, M.; Basu, K.; Benoit, C.; Cirtiu, C. M.; Vali, H.; Moores, A. Cellulose nanocrystals as chiral inducers: Enantioselective catalysis and transmission electron microscopy 3D characterization. *J. Am. Chem. Soc.* **2015**, *137*, 6124−6127.
(5) Querejeta-Fernández, A.; Chauve, G.; Methot, M.; Bouchard, J.; Kumacheva, E. Chiral plasmonic films formed by gold nanorods and cellulose nanocrystals. *J. Am. Chem. Soc.* **2014**, *136*, 4788−4793.
(6) Ivanova, A.; Fattakhova-Rohlfing, D.; Kayaalp, B. E.; Rathouský, J.; Bein, T. Tailoring the morphology of mesoporous titania thin films through biotemplating with nanocrystalline cellulose. *J. Am. Chem. Soc.* **2014**, *136*, 5930−5937.
(7) Nogi, M.; Iwamoto, S.; Nakagaito, A. N.; Yano, H. Optically Transparent Nanofiber Paper. *Adv. Mater.* **2009**, *21*, 1595−1598.
(8) Hu, L.; Zheng, G.; Yao, J.; Liu, N.; Weil, B.; Eskilsson, M.; Karabulut, E.; Ruan, Z.; Fan, S.; Bloking, J. T.; McGehee, M. D.; Wågberg, L.; Cui, Y. Transparent and conductive paper from nanocellulose fibers. *Energy Environ. Sci.* **2013**, *6*, 513−518.
(9) Si, Y.; Fu, Q.; Wang, X.; Zhu, J.; Yu, J.; Sun, G.; Ding, B. Superelastic and Superhydrophobic Nanofiber-Assembled Cellular Aerogels for Effective Separation of Oil/Water Emulsions. *ACS Nano* **2015**, *9*, 3791−3799.
(10) Toivonen, M. S.; Kaskela, A.; Rojas, O. J.; Kauppinen, E. I.; Ikkala, O. Ambient-Dried Cellulose Nanofibril Aerogel Membranes with High Tensile Strength and Their Use for Aerosol Collection and Templates for Transparent, Flexible Devices. *Adv. Funct. Mater.* **2015**, *25*, 6618−6626.
(11) Kobayashi, Y.; Saito, T.; Isogai, A. Aerogels with 3D ordered nanofiber skeletons of liquid-crystalline nanocellulose derivatives as tough and transparent insulators. *Angew. Chem., Int. Ed. Engl.* **2014**, *53*, 10394−10397.
(12) Zhu, H.; Yang, X.; Cranston, E. D.; Zhu, S. Flexible and Porous Nanocellulose Aerogels with High Loadings of Metal−Organic-Framework Particles for Separations Applications. *Adv. Mater.* **2016**, *28*, 7652−7657.
(13) Petersen, N.; Gatenholm, P. Bacterial cellulose-based materials and medical devices: current state and perspectives. *Appl. Microbiol. Biotechnol.* **2011**, *91*, 1277−1286.
(14) Nakagaito, A. N.; Iwamoto, S.; Yano, H. Bacterial cellulose: the ultimate nano-scalar cellulose morphology for the production of high-strength composites. *Appl. Phys. A* **2005**, *80*, 93−97.
(15) Osong, S. H.; Norgren, S.; Engstrand, P. Processing of wood-based microfibrillated cellulose and nanofibrillated cellulose, and applications relating to papermaking: a review. *Cellulose* **2016**, *23*, 93−123.
(16) Lindström, T. Aspects on nanofibrillated cellulose (NFC) processing, rheology and NFC-film properties. *Curr. Opin. Colloid Interface Sci.* **2017**, *29*, 68−75.
(17) Veen, S. J.; Kuijk, A.; Versluis, P.; Husken, H.; Velikov, K. P. Phase Transitions in Cellulose Microfibril Dispersions by High-Energy Mechanical Deagglomeration. *Langmuir* **2014**, *30*, 13362−13368.
(18) Hanley, S. J.; Giasson, J.; Revol, J.-F.; Gray, D. G. Atomic force microscopy of cellulose microfibrils: comparison with transmission electron microscopy. *Polymer* **1992**, *33*, 4639−4642.
(19) Hanley, S. J.; Revol, J.-F.; Godbout, L.; Gray, D. G. Atomic force microscopy and transmission electron microscopy of cellulose from Micrasterias denticulata; evidence for a chiral helical microfibril twist. *Cellulose* **1997**, *4*, 209−220.
(20) Iwamoto, S.; Kai, W.; Isogai, A.; Iwata, T. Elastic Modulus of Single Cellulose Microfibrils from Tunicate Measured by Atomic Force Microscopy. *Biomacromolecules* **2009**, *10*, 2571−2576.
(21) Clasen, C.; Sultanova, B.; Wilhelms, T.; Heisig, P.; Kulicke, W.-M. Effects of Different Drying Processes on the Material Properties of Bacterial Cellulose Membranes. *Macromol. Symp.* **2006**, *244*, 48−58.
(22) Liesche, J.; Ziomkiewicz, I.; Schulz, A. Super-resolution imaging with Pontamine Fast Scarlet 4BS enables direct visualization of cellulose orientation and cell connection architecture in onion epidermis cells. *BMC Plant Biol.* **2013**, *13*, 226.
(23) Helbert, W.; Chanzy, H.; Husum, T. L.; Schülein, M.; Ernst, S. Fluorescent cellulose microfibrils as substrate for the detection of cellulase activity. *Biomacromolecules* **2003**, *4*, 481−487.
(24) Zammarano, M.; Maupin, P. H.; Sung, L.-P.; Gilman, J. W.; McCarthy, E. D.; Kim, Y. S.; Fox, D. M. Revealing the interface in polymer nanocomposites. *ACS Nano* **2011**, *5*, 3391−3399.
(25) Zhang, W.; Zhang, Y.; Lu, C.; Deng, Y. Aerogels from crosslinked cellulose nano/micro-fibrils and their fast shape recovery property in water. *J. Mater. Chem.* **2012**, *22*, 11642−11650.
(26) Wang, M.; Anoshkin, I. V.; Nasibulin, A. G.; Korhonen, J. T.; Seitsonen, J.; Pere, J.; Kauppinen, E. I.; Ras, R. H. A.; Ikkala, O. Modifying native nanocellulose aerogels with carbon nanotubes for mechanoresponsive conductivity and pressure sensing. *Adv. Mater.* **2013**, *25*, 2428−2432.
(27) Hestrin, S.; Schramm, M. Synthesis of cellulose by *Acetobacter xylinum*. 2. Preparation of freeze-dried cells capable of polymerizing glucose to cellulose. *Biochem. J.* **1954**, *58*, 345−352.
(28) Hell, S.; Reiner, G.; Cremer, C.; Stelzer, E. H. K. Aberrations in confocal fluorescence microscopy induced by mismatches in refractive index. *J. Microsc.* **1993**, *169*, 391−405.
(29) Brown, R. M.; Willison, J. H.; Richardson, C. L. Cellulose biosynthesis in *Acetobacter xylinum*: visualization of the site of synthesis and direct measurement of the in vivo process. *Proc. Natl. Acad. Sci. U.S.A.* **1976**, *73*, 4565−4569.
(30) Fink, H.-P.; Purz, H. J.; Bohn, A.; Kunze, J. Investigation of the supramolecular structure of never dried bacterial cellulose. *Macromol. Symp.* **1997**, *120*, 207−217.
(31) Xu, T.; Vavylonis, D.; Huang, X. 3D actin network centerline extraction with multiple active contours. *Med. Image Anal.* **2014**, *18*, 272−284.
(32) MacKintosh, F. C.; Käs, J.; Janmey, P. A. Elasticity of Semiflexible Biopolymer Networks. *Phys. Rev. Lett.* **1995**, *75*, 4425−4428.
(33) de Kort, D. W.; Veen, S. J.; Van As, H.; Bonn, D.; Velikov, K. P.; van Duynhoven, J. P. M. Yielding and flow of cellulose microfibril dispersions in the presence of a charged polymer. *Soft Matter* **2016**, *12*, 4739−4744.
(34) Lin, D.; Li, R.; Lopez-Sanchez, P.; Li, Z. Physical properties of bacterial cellulose aqueous suspensions treated by high pressure homogenizer. *Food Hydrocolloids* **2015**, *44*, 435−442.
(35) Colvin, J. R. Twisting of bundles of bacterial cellulose microfibrils. *J. Polym. Sci.* **1961**, *49*, 473−477.
(36) Khandelwal, M.; Windle, A. Origin of chiral interactions in cellulose supra-molecular microfibrils. *Carbohydr. Polym.* **2014**, *106*, 128−131.
(37) Majoinen, J.; Haataja, J. S.; Appelhans, D.; Lederer, A.; Olszewska, A.; Seitsonen, J.; Aseyev, V.; Kontturi, E.; Rosilo, H.; Österberg, M.; Houbenov, N.; Ikkala, O. Supracolloidal multivalent interactions and wrapping of dendronized glycopolymers on native cellulose nanocrystals. *J. Am. Chem. Soc.* **2014**, *136*, 866−869.
(38) Sun, C. True density of microcrystalline cellulose. *J. Pharm. Sci.* **2005**, *94*, 2132−2134.
(39) Nielsen, L. J.; Eyley, S.; Thielemans, W.; Aylott, J. W. Dual fluorescent labelling of cellulose nanocrystals for pH sensing. *Chem. Commun.* **2010**, *46*, 8929−8931.
(40) Nyquist, H. Certain topics in telegraph transmission theory. *Proc. IEEE* **2002**, *90*, 280−305.
(41) Van Der Voort, H. T. M.; Strasters, K. C. Restoration of confocal images for quantitative image analysis. *J. Microsc.* **1995**, *178*, 165−181.
(42) Xu, T.; Vavylonis, D.; Tsai, F.-C.; Koenderink, G. H.; Nie, W.; Yusuf, E.; Lee, I.-J.; Wu, J.-Q.; Huang, X. SOAX: A software for quantification of 3D biopolymer networks. *Sci. Rep.* **2015**, *5*, 9081.

DOI: 10.1021/acsomega.7b00536
ACS Omega 2017, 2, 5019−5024